

# High-Capacity Framework for Reversible Data Hiding in Encrypted Image Using Pixel Predictions and Entropy Encoding

Yingqiang Qiu, Yuyan Yang, Qichao Ying, Huanqiang Zeng, *Senior Member, IEEE*, Zhenxing Qian, *Member, IEEE*

**Abstract**—Previous reversible data hiding in encrypted images (RDHEI) schemes can be either carried out by vacating room before or after data encryption, which leads to a separation of the search field in RDHEI. Besides, high capacity relies heavily on vacating room before encryption (VRBE), which significantly lowers the payload of vacating room after encryption (VRAE) based schemes. To address this issue, this paper proposes a framework for high-capacity RDHEI for both VRBE and VRAE cases using pixel predictions and entropy encoding. We propose an embedding room generation algorithm to produce vacated room by generating the prediction-error histogram (PEH) of the selected cover using adjacency prediction and the median edge detector (MED). In the VRBE scenario, we propose a scheme that generates the embedding room using the proposed algorithm, and encrypts the preprocessed image by using the stream cipher with two encryption keys. In the VRAE scenario, we propose a scheme that involves an improved block modulation and permutation encryption algorithm where the spatial redundancy in the plain-text image can be largely preserved. Then the proposed algorithm is applied on the encrypted image to generate the embedding room. At the data hider's side of both the schemes, the data hider locates the embedding room and embeds the encrypted additional data. On receiving the marked encrypted image, the receivers with different authentication can respectively conduct error-free data extraction and/or error-free image recovery. The experimental results show that the two schemes in the proposed framework can outperform many previous state-of-the-art RDHEI arts. Besides, the proposed schemes can ensure high information security in that little detail of the original image can be directly discovered from the encrypted images or the marked encrypted images.

**Index Terms**—Reversible data hiding, encrypted image, entropy encoding, image trust, copyright protection

## I. INTRODUCTION

Reversible data hiding (RDH) has the capability of accurately recovering the cover medium after the hidden data is extracted. For this reason, RDH is widely applied in some important and sensitive applications, i.e., covert communication, data hiding for medical images and law-enforcement, etc. In the past two decades, many RDH

This work was supported by the Natural Science Foundation of China (Grant U20B2051, 61972168, 61871434). Corresponding author: Zhenxing Qian.

Y. Qiu, Y. Yang and H. Zeng are with the College of Information Science & Engineering, Huaqiao University, Xiamen 361021, China. (e-mail: yqqiu@hqu.edu.cn, yyy@xmut.edu.cn, zeng0043@hqu.edu.cn).

researches have been done, most of which are developed for uncompressed images. Traditionally, RDH focuses on enlarging the embedding capacity and minimizing the distortion with the criterion of the peak signal-to-noise ratio (PSNR). Typical RDH schemes can be classified into three categories, i.e., difference expansion (DE) based RDH [1-4], histogram shifting (HS) based RDH [5-8], and entropy coding based RDH [9-11]. In addition, there are many RDH schemes for JPEG images [12-15].

With the growing development of remote service, cloud security has attracted considerable attentions. For data privacy protection, the encryption technique is widely used in cloud systems. In many applications, the cloud server needs to embed some additional data into the encrypted multimedia, such as the copyright data, timestamp, etc. However, the spatial redundancy of the cover multimedia is largely reduced during encryption. As a result, the traditional RDH methods are generally not efficient for the encrypted images. Therefore, in recent years, RDH in encrypted images (RDHEI) has attracted extensive research interest.

Fig.1 depicts the general framework of RDHEI. Typically, there are three parties involved in the data flow, i.e., the image owner, the data hider, and the receiver. The image owner first encrypts the cover image with or without some image preprocessing, namely, whether the owner generates embedding room before image encryption, and uploads the encrypted image onto the cloud. Then, the cloud server, also the data hider, embeds some additional data into the encrypted image. Finally, the receiver with different authentication can extract the embedded data error-free and/or recover the original image losslessly.

The existing RDHEI methods can be divided into two categories by different application scenarios: vacating room after encryption (VRAE) [16-24] and vacating room before encryption (VRBE) [25-37]. The main difference lies in that whether in the application, the image owner can vacate the embedding room ahead of image encryption. VRBE-based methods allow the image owner to vacate the embedding room

Q. Ying and Z. Qian are with Shanghai Institute of Intelligent Electronics & Systems, School of Computer Science, Fudan University, Shanghai 200433, China (e-mail: shinydotcom@163.com, zxqian@fudan.edu.cn).

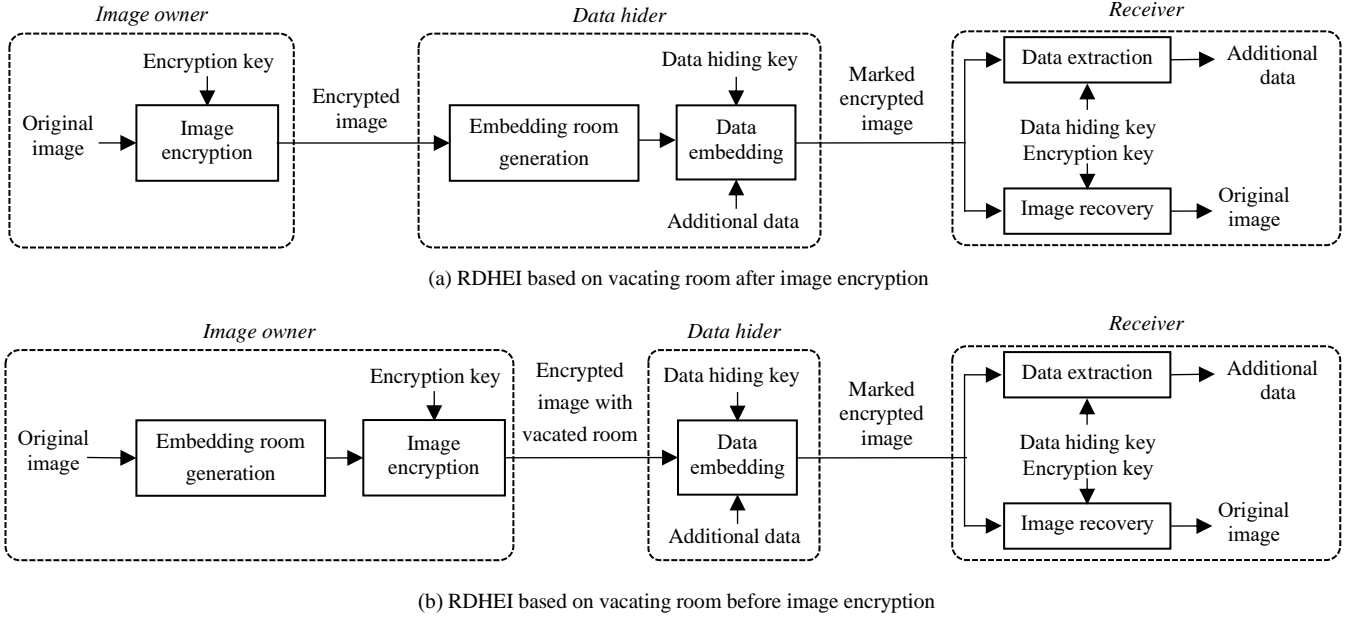


Fig. 1. The general frameworks for RDHEI (a) VRAE (b) VRBE

ahead of image encryption. Therefore, spatial redundancy in the original image can be exploited so that a large amount of embedding room can be reserved and efficiently utilized for data embedding. However, in many real-world applications, VRBE is not allowed in that the image owner does not know the fact that the server needs to embed secret data into the image. Therefore, the owner may not assist the data hider by conducting image preprocessing. It gives rise to the VRAE-based RDHEI schemes where the image owner directly encrypts the cover image and does not reserve any direct information about the original image. Therefore, the remote server can only generate the embedding room by modified some pixel values of the encrypted image. The state-of-the-art VRAE methods can achieve decent performances of RDH in encrypted image. But since the entropy of the encrypted image is usually maximized because of image encryption, the net payloads of these methods are significantly lower than those of VRBE.

Though both VRAE-based and VRBE-based methods can provide promising embedding performances, there still remains many problems. First, as mentioned above, high capacity relies heavily on vacating room before encryption, which lowers the payload of VRAE-based schemes. Second, many efficient embedding strategies proposed for one category cannot be efficiently applied on the other category, which leads to a separation of the search field in RDHEI. Third, many state-of-the-art methods from both the categories cannot embed a large payload into textured images, and there are also some security flaws. Therefore, it is urgent to develop a framework that can work on both VRAE and VRBE scenario and provide high embedding payload. It also leaves room for developing novel RDHEI schemes with better security and higher payload for textured images as well.

This paper proposes a framework for high-capacity RDHEI for both VRBE and VRAE cases using pixel prediction and entropy encoding. We denote the proposed scheme as PE-

VRBE and PE-VRAE, respectively. We begin with proposing an embedding room generation algorithm to produce vacated room by generating the prediction-error histogram (PEH) of the selected cover using adjacency prediction and the median edge detector (MED). According to the prediction errors, we divide the pixels into independently encoding pixels and jointly encoding pixels. We then compress prediction errors with arithmetic encoding and conduct self-embedding. This way, high-capacity embedding room can be generated for RDHEI. In the VRBE scenario, we apply the proposed algorithm on the plain-text cover image to generate the embedding room. Then the owner encrypts the preprocessed image by using the stream cipher, which can avoid the content leakage of cover image. At the data hider's side, the data hider locates the vacated room and embed the encrypted additional data. In the VRAE scenario, the image owner firstly encrypts the cover image by block modulation based on the context of adjacent block and block permutation. The spatial redundancy in the plain-text image can be largely preserved within image blocks after the encryption. Afterwards, we apply the proposed algorithm on the encrypted blocks. The data hider can similarly find the vacated room and embed his information. At the recipient's side, error-free data extraction and error-free image recovery can be respectively conducted in an inversed way, and both of the two proposed schemes are separable, namely, the receivers with different authentication get different results. Experimental results of the proposed framework demonstrate that the proposed schemes can achieve much higher embedding capacity compared to many state-of-the-art RDHEI methods. At the same time, the proposed scheme can provide high information security.

The main contributions of this paper are three-folded:

- We are the first to propose a RDHEI framework that can both work on VRAE and VRBE cases
- The proposed schemes in the framework are high in payload, which can beat state-of-the-art RDHEI schemes.

- Less detail of the original image can be discovered from the encrypted image by the unauthorized users. Besides, the proposed framework can provide large payload for textured images.

The remainder of this paper is organized as follows: Section II introduces the related works. The proposed embedding room generation algorithm is detailed in Section III. The proposed VRBE-based scheme and VRAE-based scheme is then introduced in Section IV and Section V, respectively. Experimental results and discussions are provided in Section VI. Section VII discusses the extension of Huffman encoding and Section VIII concludes this paper.

## II. RELATED WORKS

### A. Vacating Room After Encryption (VRAE)

Puech et al. proposed the first RDHEI scheme [16], where the data hider vacated the embedding room within the encrypted version of the cover image. Since then, VRAE-based RDHEI schemes have received extensive attentions. In [17], Zhang firstly encrypted the cover image using the stream cipher. Then, each selected block of encrypted image can accommodate one bit by flipping or keeping three LSBs of all pixels in the block. The corresponding data extraction and image recovery were operated by observing the block smoothness. However, with the block size decreases, namely, the amount of embedded data increases, extracted-bit errors may occur during data extraction and image recovery. To decrease the extracted-bit error rate, Hong et al. [18] improved this method by using a side match mechanism for measuring the smoothness of blocks. Zhou et al. [19] proposed to embed additional data in the encryption domain by using a public key modulation mechanism, and designed a two-class SVM classifier to distinguish encrypted and nonencrypted image patches at the decoding side. In these VRAE-based methods [17-19], each image block can accommodate one bit, and therefore the achieved embedding capacity is relatively small. Besides, the operation of data extraction and image recovery should be done jointly after marked image decryption. But the scheme may also have errored bits after data extraction.

Some researchers also proposed separable VRAE-based RDHEI schemes. The first RDHEI scheme [16] is separable, where the embedded data is extracted before the image decryption and the original image is recovered after decryption. In [20], Zhang further proposed a separable RDHEI method for stream-enciphered images, where the encrypted image was divided into blocks, and the LSBs of each block were compressed to generate embedding room for additional data. By using low density parity check codes (LDPC), Qian et al. [21] compressed the selected bits taken from the stream-ciphered image into syndrome bits, vacating room to accommodate some additional data. In [22], original image was encrypted by public key cryptosystems with probabilistic and homomorphic properties. Base on the benefit of the homomorphic encryption, lossless and reversible data hiding can be achieved in the image encryption domain. Since the entropy of an encrypted image is

generally high, the achieved embedding capacities of these VRAE-based methods [16-22] are relatively small. In [23], Yi et al. proposed a separable VRAE-based RDHEI method with high embedding capacity. The image owner firstly divided the cover image into non-overlapping blocks, and then encrypted it with block permutation and co-modulation (BPCM). The spatial redundancy of each image block was preserved well in a certain extent. After the encrypted image was uploaded to the cloud, the data hider was able to embed a larger amount of additional data into encrypted image by using parametric binary tree labeling (PBTL).

There is still room for [23] to achieve higher embedding capacity. For example, the spatial redundancy of each image block can be reserved better during image encryption in that pixels are predicted with one special pixel in the same block does not take full use of the reserved spatial redundancy. Also, the efficiency of entropy coding can be improved by replacing PBTL with a more efficient entropy coding method. Besides, Qu et al. [24] analysed the security of the RDHEI algorithm based on BPCM encryption under known plaintext attacks (KPAs), and showed that BPCM encryption has the risk of information leakage.

### B. Vacating Room Before Encryption (VRBE)

Different from VRAE-based methods, VRBE-based methods allow the image owner to vacate the embedding room ahead of image encryption. Therefore, spatial redundancy in the original image can be exploited so that a higher embedding capacity can be achieved. Ma et al. [25] proposed the first VRBE-based RDHEI scheme based on histogram shifting. A considerable amount of vacated room can be reserved by the image owner and further utilized by the data hider. The work receives extensive attentions and many improved schemes are proposed. In [26], Zhang et al. proposed to embed additional data into the prediction errors of some selected pixels to generate embedding room before image encryption. In [27], the prediction errors generated by interpolation techniques were encrypted by a novel mode. In [28], the embedding room was vacated by using patch-level sparse representation before image encryption. And RDH for homomorphic encrypted image vacated room by self-embedding [29]. However, the embedding capacity is still relatively low.

To further increase the payload of RDHEI, Qiu et al. [30] performed block-wise adaptive reversible integer transformation (ARIT) on the original image, and a large amount of embedding room can be vacated in the LSBs of transformed image blocks. Similarly, Qiu et al. [31] proposed a RDHEI method based on ARIT, where high embedding capacity can be provided for both the image owner and the cloud server. Puteaux et al. proposed two RDHEI approaches [32] based on MSB prediction, i.e., high-capacity reversible data hiding approach with correction of prediction errors (CPE-HCRDH) and high-capacity reversible data hiding approach with embedded prediction errors (EPE-HCRDH). Base on the PBTL proposed in [23], Wu et al. [33] used the redundancy of the entire plain-text image instead of the encrypted image blocks to vacate a larger embedding room before image encryption.

Table 1. Pixels' assignment by using MED predictor for image block sized  $n=4\times 4$ 

$a$	$b$	$c$	$y$	$a$	$b$	$c$	$y$	$a$	$b$	$c$	$y$
$y_{i,2,2}$	$y_{i,2,1}$	$y_{i,1,2}$	$y_{i,1,1}$	$y_{i,2,2}$	$y_{i,2,3}$	$y_{i,1,2}$	$y_{i,1,3}$	$y_{i,2,3}$	$y_{i,2,4}$	$y_{i,1,3}$	$y_{i,1,4}$
$y_{i,2,2}$	$y_{i,2,1}$	$y_{i,3,2}$	$y_{i,3,1}$	$y_{i,2,2}$	$y_{i,2,3}$	$y_{i,3,2}$	$y_{i,3,3}$	$y_{i,2,3}$	$y_{i,2,4}$	$y_{i,3,3}$	$y_{i,3,4}$
$y_{i,3,2}$	$y_{i,3,1}$	$y_{i,4,2}$	$y_{i,4,1}$	$y_{i,3,2}$	$y_{i,3,3}$	$y_{i,4,2}$	$y_{i,4,3}$	$y_{i,3,3}$	$y_{i,3,4}$	$y_{i,4,3}$	$y_{i,4,4}$

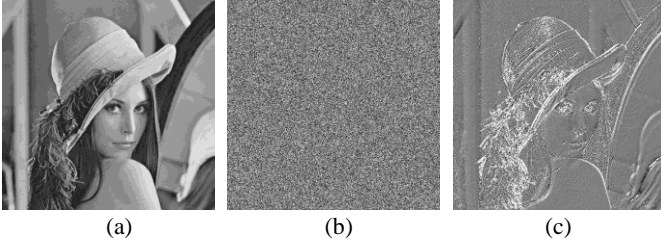


Fig. 2. The security flaw of method [33]

Chen et al. [34] used the correlations of high bit-planes of the plain-text image by compressing the MSB planes of plain-text images, which was improved by Yin et al. [35] by using both pixel prediction and high bit-planes compression of prediction errors to achieve a higher embedding capacity. Besides, Yin et al. [36] further proposed a high-capacity RDHEI scheme based on multi-MSB prediction and Huffman encoding. Compared with [25-29], [30-36] can achieve much higher embedding capacity.

Though promising in the embedding performances, many state-of-the-art VRBE-based methods cannot embed a large payload into textured images. Besides, there are some security flaws in current methods, i.e., the security of the RDHEI by MSB prediction of [32] was investigated in [37], where solutions to circumvent the security flaws at similar bit-rates and mathematical complexity were proposed. In [33], a fingerprint of the cover image can still be obtained from the PBTL in encryption domain, which directly corresponds to its prediction error histogram. Any potential attacker can extract prediction errors from the encrypted image to get the content of cover image. As showed in Fig. 2, (a) is the original image Lena sized  $512\times 512$ ; (b) is the marked encrypted image of (a) with RDHEI method in [33], where  $\alpha = 5$ ,  $\beta = 2$  and the embedding rate (ER) is  $2.645\text{bpp}$ (bits per pixel); (c) is the resulted image obtained from the PBTLs of (b), where the detected prediction errors in  $[-11, 12]$  are mapped to  $[0,255]$  for better visibility as an image. From Fig. 2 (c), contour lines of (a) are clearly visible, the marked encrypted image can be identified.

### III. EFFICIENT EMBEDDING ROOM GENERATION ALGORITHM

We begin with introducing a novel efficient embedding room generation algorithm for RDHEI. We denote the targeted image before embedding room generation as  $\mathbf{Y}$ . In VRBE,  $\mathbf{Y}$  is the plain-text image, while in VRAE,  $\mathbf{Y}$  is the encrypted image (discussed in Section V.A). Without loss of generality, we assume that  $\mathbf{Y}$  is an 8-bits gray-scaled image with a size of  $N_1 \times N_2$ . The proposed algorithm is composed of three steps: generation of the prediction-error histogram, optimal entropy encoding, and embedding room generation by self-embedding. In addition, we discuss the data recovery procedures using entropy decoding.

#### A. Prediction Errors Generation

Firstly, we make predictions on the pixels by using adjacency prediction and the MED predictor. Assume that  $Y_i$  is the non-overlapping image blocks sized  $n = n_1 \times n_2$ , and therefore the amount of blocks is  $N = \lfloor N_1/n_1 \rfloor \times \lfloor N_2/n_2 \rfloor$ ,  $1 \leq i \leq N$ .

For each block  $Y_i$ , we select one pixel  $y_{i,j_1,k_1}$  ( $1 \leq j_1 \leq n_1$ ,  $1 \leq k_1 \leq n_2$ ) as the **reference pixel** ( $P_R$ ), and the other pixels as the **embedding pixels** ( $P_E$ ), which can be predicted as follows:

(1) For pixels in horizontal direction of  $y_{i,j_1,k_1}$ ,

$$py_{i,j_1,k} = \begin{cases} y_{i,j_1,k+1}, & 1 \leq k < k_1 \\ y_{i,j_1,k-1}, & k_1 < k \leq n_2 \end{cases} \quad (1)$$

(2) For pixels in vertical direction of  $y_{i,j_1,k_1}$ ,

$$py_{i,j,k_1} = \begin{cases} y_{i,j+1,k_1}, & 1 \leq j < j_1 \\ y_{i,j-1,k_1}, & j_1 < j \leq n_1 \end{cases} \quad (2)$$

(3) For other pixels in upper left, upper right, bottom left or bottom right side of  $y_{i,j_1,k_1}$ , the value is predicted by MED predictor. Accordingly, four MED prediction templates are showed in Fig. 3, where  $y$  represents the pixel needed to be predicted, and the neighboring pixels of  $y$  are denoted by  $a$ ,  $b$  and  $c$  respectively. The prediction value  $py$  of  $y$  is predicted by:

$$py = \begin{cases} \max(b, c), & a \leq \min(b, c) \\ \min(b, c), & a \geq \max(b, c) \\ b + c - a, & \text{otherwise} \end{cases} \quad (3)$$

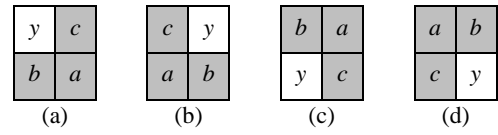
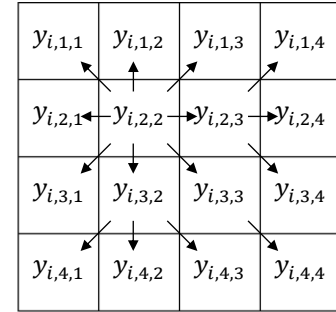


Fig.3 Four prediction templates for MED

Fig. 4 Example of pixel prediction for image block sized  $n=4\times 4$ 

In this way,  $(n - 1)$  predicted values can be obtained in each image block. Take image block sized  $n = 4 \times 4$  as an example, in Fig. 4, we regard  $y_{i,2,2}$  as the reference pixel, the other pixels are predicted by the following:

- (1) on the horizontal direction,  $y_{i,2,1}$  and  $y_{i,2,3}$  are predicted with  $y_{i,2,2}$ ,  $y_{i,2,4}$  is predicted with  $y_{i,2,3}$ ;
- (2) on the vertical direction,  $y_{i,1,2}$  and  $y_{i,3,2}$  are predicted with  $y_{i,2,2}$ ,  $y_{i,4,2}$  is predicted with  $y_{i,3,2}$ ;
- (3) on the corners, the pixels of  $a, b, c$  and  $y$  are showed in Table 1.

Afterwards, the prediction error  $e_{i,j,k}$  can be calculated by

$$e_{i,j,k} = y_{i,j,k} - py_{i,j,k}, \quad (4)$$

where  $e_{i,j,k} \in [-255, 255]$ ,  $j \neq j_1$  or  $k \neq k_1$ . Hence,  $N \cdot (n - 1)$  prediction errors are obtained.

After calculating all prediction-errors  $e_{i,j,k}$ , we construct the prediction-error histogram (PEH) represented as  $h$  in (5).

$$h = \{h_e | h_e = \#(e_{i,j,k} = e), e \in [-255, 255]\}, \quad (5)$$

where  $\#$  denotes the amount of satisfied prediction errors. The prediction-error histogram is denoted as  $h = \{h_{-255}, h_{-254}, \dots, h_{-1}, h_0, \dots, h_{254}, h_{255}\}$ . The reference pixels are excluded from  $h$ .

### B. Optimized Entropy Encoding

For plain-text images in VRBE, PEH generally obeys the Laplacian-like distribution centered at zero, that is the value of  $h_e$  decreases along with the absolute value of  $e$  increases. Since the spatial correlation can be well preserved within each encrypted image block, the obtained PEH in VRAE also generally obeys the Laplacian-like distribution centered at zero.

We separate the histogram bins  $\{h_{-255}, h_{-254}, \dots, h_{-1}, h_0, \dots, h_{254}, h_{255}\}$  of the PEH into two categories: independent encoding bins  $B_I = \{h_{-T}, h_{-T+1}, \dots, h_{-1}, h_0, \dots, h_{T-2}, h_{T-1}\}$  and joint encoding bins  $B_J = \{h_{-255}, h_{-254}, \dots, h_{-T-2}, h_{-T-1}, h_T, h_{T+1}, \dots, h_{254}, h_{255}\}$ ,  $h = B_I \cup B_J$ .  $T$  is an adaptive threshold that alters with the PEH, i.e., different cover images use different  $T$  for highest payload. Accordingly, we define the embedding pixels as **independent encoding pixels** ( $P_I$ ), or **jointly encoding pixels** ( $P_J$ ). By the way, all prediction errors are classified into  $(2T+1)$  categories, which can be losslessly compressed with traditional entropy-coding methods, set the length of compressed data ( $CD$ ) to be  $\ell_T(CD)$ . Since the pixels in  $P_J$  are jointly encoded, their original values should be kept as auxiliary data ( $AD$ ) for image recovery, whose length is

$$\ell_T(AD) = 8h_J, \quad (6)$$

where,  $h_J = \sum_{e=-255}^{-T-1} h_e + \sum_{e=T}^{255} h_e$ . To achieve real data embedding, the total length  $L$  of the compressed data and auxiliary data should satisfy

$$L = \ell_T(CD) + \ell_T(AD) < 8N(n_1 n_2 - 1) < 8N_1 N_2, \quad (7)$$

which needs to be recorded with  $\ell(L)$  bits, and

$$\ell(L) = 3 + \lceil \log_2 N_1 \rceil + \lceil \log_2 N_2 \rceil, \quad (8)$$

$\lceil \cdot \rceil$  is the ceil function. Therefore, the embedding capacity of vacated room is

$$\begin{aligned} EC_T &= 8 \cdot \sum_{e=-255}^{255} h_e - \ell_T(CD) - \ell_T(AD) - \ell(L) \\ &= 8 \cdot \sum_{e=-T}^{T-1} h_e - \ell_T(CD) - \ell(L) \end{aligned} \quad (9)$$

For special image  $\mathbf{Y}$ ,  $\ell(L)$  is a constant. To achieve higher embedding capacity, we should adapt an efficient lossless

compression algorithm and find out the optimal threshold  $T_{opt}$  to decrease the total length of the compressed data and auxiliary data. For a specific image  $\mathbf{Y}$ , different thresholds and different compression algorithms lead to different entropy encoding results. With special entropy coding method, the operator determines  $T_{opt}$  by trying  $T \in [1, 255]$ , and select the optimized one with the largest amount of vacated room as  $T_{opt}$ . To this end, we discuss arithmetic coding as follow.

Arithmetic coding (AC) is a kind of typical entropy encoding method used in lossless data compression, which encodes the entire pixels into a single number, an arbitrary-precision fraction  $f$ , where  $0.0 \leq f < 1.0$ .

For a given  $T \in [1, 255]$ , the **independent encoding pixels** with the same prediction error  $e \in [-T, T - 1]$  are assigned with an independent symbol, all **jointly encoding pixels** are assigned with a same symbol. Therefore, the amount of  $(2T+1)$  symbols is  $\{h_{-T}, h_{-T+1}, \dots, h_{-1}, h_0, \dots, h_{T-2}, h_{T-1}, h_J\}$  respectively, which should be recorded for data decompression. Since it is less than the total num of pixels  $N_1 \times N_2$ , the amount of each symbol can be expressed within  $(\lceil \log_2 N_1 \rceil + \lceil \log_2 N_2 \rceil)$  bits. To achieve real data embedding, the length of output data with arithmetic encoding should be less than  $8 \cdot N_1 \cdot N_2$ , which can be denoted within  $(3 + \lceil \log_2 N_1 \rceil + \lceil \log_2 N_2 \rceil)$  bits. For  $T \in [1, 255]$ , it can be expressed within eight bits. Thus, the above side information is concatenated as a binary sequence with length  $\ell_T(CD_1)$  as

$$\ell_T(CD_1) = 11 + (2T+2) \cdot (\lceil \log_2 N_1 \rceil + \lceil \log_2 N_2 \rceil) \quad (10)$$

Then, the occurrence of each symbol for  $e \in [-T, T - 1]$  can be calculated as

$$p_e = h_e / \sum_{e=-255}^{255} h_e. \quad (11)$$

The total occurrence of the symbol for  $P_J$  is

$$p_J = 1 - \sum_{e=-T}^{T-1} p_e \quad (12)$$

With  $\{p_{-T}, p_{-T+1}, \dots, p_{-1}, p_0, \dots, p_{T-2}, p_{T-1}, p_J\}$ , all symbols assigned for all **embedding pixels** can be compressed entirely to be a binary sequence  $CD_2$  with length  $\ell_T(CD_2)$ . Then,  $CD_1$  is appended with  $CD_2$ , we have

$$\ell_T(CD) = \ell_T(CD_1) + \ell_T(CD_2) = 11 + \ell_T(CD') \quad (13)$$

where,

$$\ell_T(CD') = (2T+2) \cdot (\lceil \log_2 N_1 \rceil + \lceil \log_2 N_2 \rceil) + \ell_T(CD_2). \quad (14)$$

With arithmetic coding, the embedding capacity of vacated room in (9) can be described as

$$EC_T = 8 \cdot \sum_{e=-T}^{T-1} h_e - 11 - \ell(L) - \ell_T(CD') \quad (15)$$

Then, to achieve maximal embedding capacity, optimal thresholds  $T_{opt}$  should satisfy

$$T_{opt} = \operatorname{argmax}_{T \in [1, 255]} EC_T \quad (16)$$

### C. Embedding Room Generation using Self-embedding

With arithmetic coding, we can compress the **embedding pixels** of image  $\mathbf{Y}$  to be  $CD$  and  $AD$ . Skipping all reference pixels, we replace the first  $\ell(L)$  bits in the LSB-plane of all embedding pixels with the value of  $L$ , which can be encrypted if needed in application. Subsequently, the lower bit-planes of all embedding pixels are replaced by the binary sequence of  $CD$  and  $AD$ , which also can be encrypted if needed. The other higher bit-planes of all embedding pixels are vacated for data

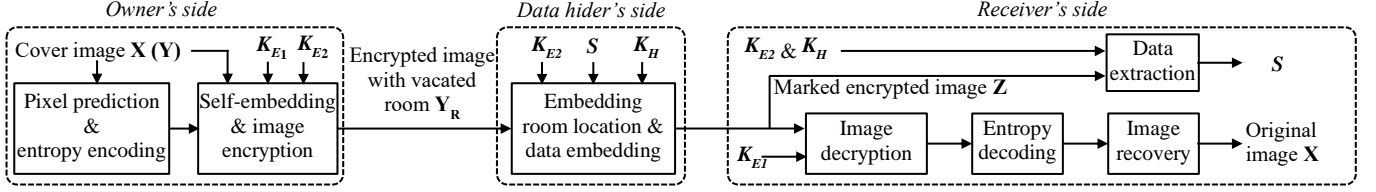


Fig. 5. The frameworks of the proposed PE-VRBE RDHEI scheme

embedding in the image encryption domain, and  $L$  indicates the embedding room for the authorized data hider or receiver. The resulted image is an image with vacating room, which can be denoted as  $\mathbf{Y}'$ .

#### D. Data Recovery Using Entropy Decoding

From the image with vacating room  $\mathbf{Y}'$ , we skip the all referenced pixels and the first  $\ell(L)$  bits in the LSB-plane of all embedding pixels. We obtain  $T_{opt}$  value from the next 8 bits in the lower bit-planes.

With  $T_{opt}$ , the amount  $\{h_{-T}, h_{-T+1}, \dots, h_{T-2}, h_{T-1}, h_J\}$  of each symbol for every  $e \in [-T, T-1]$  or all  $P_J$  can be determined by every following  $(\lceil \log_2 N_1 \rceil + \lceil \log_2 N_2 \rceil)$  bits in the lower bit-planes of all embedding pixels, and the length  $\ell(CD_2)$  is determined by the next  $(3 + \lceil \log_2 N_1 \rceil + \lceil \log_2 N_2 \rceil)$  bits. We then take the following  $\ell(CD_2)$  as the compressed data stream  $CD_2$ . After calculating  $\{p_{-T}, p_{-T+1}, \dots, p_{T-2}, p_{T-1}, p_J\}$  with  $\{h_{-T}, h_{-T+1}, \dots, h_{T-2}, h_{T-1}, h_J\}$ , we obtain the prediction errors of all embedding pixels by arithmetic decoding. Then, with the determined  $h_J$ , the auxiliary data  $AD$  is recovered.

After entropy decoding, all **jointly encoding pixels**  $P_J$  can be recovered losslessly with extracted  $AD$ . For each  $y_{i,j,k} \in P_I$  of each image block, the corresponding prediction error  $e_{i,j,k}$  is identified through entropy decoding. And then, with  $P_R$  and recovered  $P_J$ , the prediction value  $py_{i,j,k}$  can be obtained pixel by pixel as Section III.A, and then its original value  $y_{i,j,k}$  can be recovered with (17),

$$y_{i,j,k} = e_{i,j,k} + py_{i,j,k}. \quad (17)$$

the recovered  $P_I$  may be used to predict follow-up unrecovered  $P_I$ . This way, the original encrypted pixel values of all  $P_I$  are recovered. As a result, the image  $\mathbf{Y}$  is recovered losslessly.

## IV. THE PROPOSED VRBE-BASED RDHEI SCHEME

Fig.5 depicts the architecture of the proposed VRBE-based RDHEI scheme (PE-VRBE). The scheme contains three parts: 1) *the owner's side*, where the embedding room is vacated in the original image  $\mathbf{X}$  ( $\mathbf{Y}$  in Section III) by self-embedding, and the encrypted image with vacated room  $\mathbf{Y}_R$  is produced. 2) *the data hider's side*, where the additional data  $S$  is encrypted and embedded into  $\mathbf{Y}_R$ , and 3) *the receiver's side*, where data extraction and image recovery are separately done by the authorized users.

#### A. Image Encryption with Vacating Room

At the owner's side, the image owner selects one pixel of the original image  $\mathbf{X}$  (denoted as  $\mathbf{Y}$  in Section III) as the reference pixel, the default reference pixel is the pixel in the first row and the first column of  $\mathbf{Y}$ . Take  $\mathbf{Y}$  as an image block  $Y_1$  ( $n_1 = N_1$ ,  $n_2$

$= N_2$ ), by using adjacency prediction and MED predictor as discussion in Section III, the prediction errors histogram is generated.

Secondly, with arithmetic coding, the owner finds out the optimal threshold  $T_{opt}$ , then compresses the prediction errors losslessly to obtain the compressed data  $CD$  and auxiliary data  $AD$ , and calculate  $L = \ell(CD) + \ell(AD)$  with length  $\ell(L)$ .

Then, skipping the reference pixel and the first  $\ell(L)$  bits in the LSB-plane, the owner replaces the lower bit-planes with the compressed data and auxiliary data. As a result, the rest of the bit-planes are vacated as the embedding room. The processed image can be denoted as  $\mathbf{V}$ .

After self-embedding the compressed data into the cover image, the owner encrypts  $\mathbf{V}$  to obtain the encrypted version  $\mathbf{V}'$  using the stream cipher. A gray value  $v_{j,k}$  ( $1 \leq j \leq N_1$ ,  $1 \leq k \leq N_2$ ) in  $\mathbf{V}$  can be represented by eight bits using modulo-2 as  $v_{j,k,l}$ ,  $0 \leq l \leq 7$ .

$$v_{j,k,l} = \lfloor v_{j,k} / 2^l \rfloor \bmod 2 \quad (18)$$

where,  $\lfloor \cdot \rfloor$  stands for the floor function. The owner generates pseudo-random sequence  $P$  with the same size of the cover image according to (19). The encryption key  $K_{E1}$  is used as the seed of the pseudo-random generator.

$$P = \{p_{j,k} | p_{j,k} \in [0, 255], 1 \leq j \leq N_1, 1 \leq k \leq N_2\} \quad (19)$$

Each  $p_{j,k}$  can also be represented by eight bits using modulo-2 as,  $p_{j,k,l}$ ,  $0 \leq l \leq 7$ .

$$p_{j,k,l} = \lfloor p_{j,k} / 2^l \rfloor \bmod 2 \quad (20)$$

Then, the image owner uses the bit-wise exclusive-or (XOR) function for image encryption as

$$v_{j,k,l}' = v_{j,k,l} \oplus p_{j,k,l} \quad (21)$$

where “ $\oplus$ ” is the XOR function, and  $v_{j,k,l}'$  is the encrypted bit. Then, the encrypted pixels  $v_{j,k}'$  can be calculated as

$$v_{j,k}' = \sum_{l=0}^7 v_{j,k,l}' \cdot 2^l \quad (22)$$

Therefore, the encrypted image  $\mathbf{V}'$  is generated by the stream cipher where  $K_{E1}$  is required as the image encryption key.

With encryption key  $K_{E2}$  and stream cipher, the total length  $L$  of the compressed data and auxiliary data can be encrypted to obtain  $L'$ .  $K_{E2}$  is distributed to the authorized data hider and receiver, without which the embedding room cannot be located. Finally, the owner embeds  $L'$  into  $\mathbf{V}'$  by replacing the first  $\ell(L)$  bits in the LSB-plane of  $\mathbf{V}'$  to obtain the encrypted image with vacated room  $\mathbf{Y}_R$ .

#### B. Data Embedding

In the cloud, the data hider receives an encrypted image with vacated room  $\mathbf{Y}_R$ . The data hider skips the reference pixel and

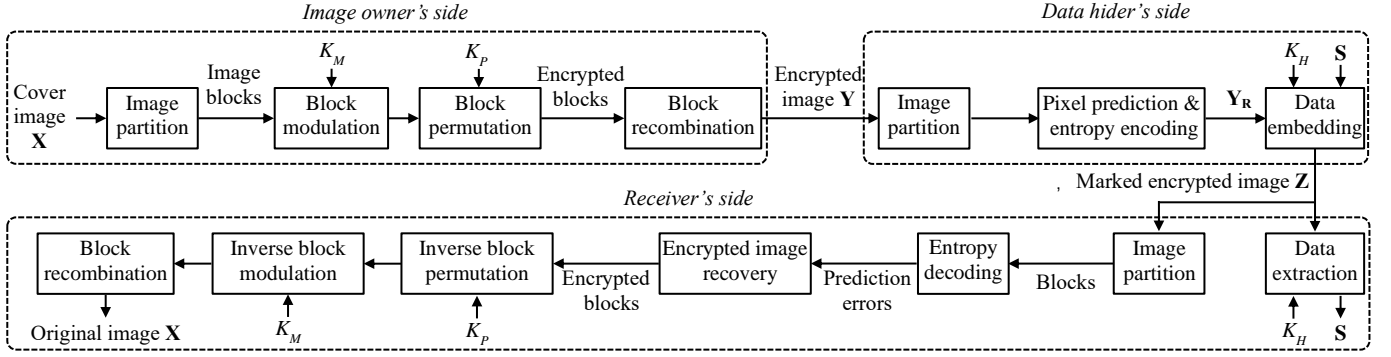


Fig. 6. The frameworks of the proposed PE-VRAE RDHEI scheme

extracts the first  $\ell(L)$  bits in the LSB-plane of  $\mathbf{Y}_R$ , then the obtained are decrypted with encryption key  $K_{E2}$ , the length  $L$  of the compressed data and auxiliary data is determined.

Then, the additional data  $\mathbf{S}$  to be embedded is encrypted with data hiding key  $K_H$ , denoted as  $\mathbf{S}'$ . With  $L$ , the hider skips the lower bit-planes carrying  $CD$  and  $AD$ , and replaces the higher bit-planes with  $\mathbf{S}'$ . This way, the marked encrypted image  $\mathbf{Z}$  based on VRBE is generated.

### C. Data Extraction and Image Recovery

At the recipient side, the process of data extraction and image recovery can be conducted separately. The authorized receiver can extract the embedded data with the data hiding key and/or recover the original image with the encryption keys respectively.

Skipping the reference pixel, the authorized receiver firstly extracts the first  $\ell(L)$  bits in the LSB-plane of  $\mathbf{Z}$ , and then decrypts the extracted data with  $K_{E2}$  to obtain the value of  $L$ . Then, With  $L$ , the receiver can skip the reference pixels and the lower bit-planes carrying  $CD$  and  $AD$ , and extract the embedded data  $\mathbf{S}'$  from the higher bit-planes. Finally, the authorized receiver with data hiding key  $K_H$  decrypts  $\mathbf{S}'$  to obtain the additional data  $\mathbf{S}$  error-free.

Since the compressed data  $CD$  and auxiliary data  $AD$  are encrypted with the image encryption key  $K_{E1}$ . With  $K_{E1}$ , the receiver decrypts  $\mathbf{Z}$  to  $\mathbf{Z}'$ . As a result, the  $CD$  and  $AD$  can be recovered error-free in the lower bit-planes of  $\mathbf{Z}'$ , and the reference pixel is recovered exactly. Then, according to Section III.D, the receiver can recover the original image  $\mathbf{Y}$ , namely,  $\mathbf{X}$  losslessly.

Only with  $K_{E2}$  and  $K_H$ , the receiver is capable to extract the embedded data  $\mathbf{S}$  error-free. Only with  $K_{E1}$ , the receiver can recover the original image losslessly. With all of the above three keys, he is capable to not only extract  $\mathbf{S}$  exactly, but also recover the cover image losslessly.

## V. THE PROPOSED VRAE-BASED RDHEI SCHEME

Fig. 6 depicts an overview of the proposed VRAE-based RDHEI scheme (PE-VRAE). The scheme is consisted of three phases: 1) the image owner's side, where the cover image  $\mathbf{X}$  is encrypted as  $\mathbf{Y}$  by block modulation and permutation, 2) the data hider's side, where the additional data  $\mathbf{S}$  is embedded into  $\mathbf{Y}$  to generate the marked encrypted image  $\mathbf{Z}$ , and 3) the

receiver's side, where the embedded data can be extracted error-free and/or the original image can be recovered losslessly. Without loss of generality, we set  $\mathbf{X}$  as the 256-level grayscale cover image sized  $N_1 \times N_2$ .

At the first phase, the image owner divides the cover image  $\mathbf{X}$  into non-overlapping blocks. Then, based on context of adjacent block, a random data is generated for the modulation of each block with encryption key  $K_M$ . After block modulation, all blocks are permuted with the encryption key  $K_P$ . By recombining all encrypted blocks, the encrypted image  $\mathbf{Y}$  is generated, which is uploaded to the cloud.

At the second phase, the data hider divides  $\mathbf{Y}$  into the blocks under the same principle. He then conducts pixel prediction within each block to obtain prediction errors. The prediction errors are grouped and compressed with optimal arithmetic encoding to vacate the embedding room. Finally, the additional data  $\mathbf{S}$  is encrypted with the data hiding key  $K_H$  and embedded into the vacated room. Therefore, the marked encrypted image  $\mathbf{Z}$  is generated.

At the last phase, after image partition, the receiver with  $K_H$  can extract the embedded additional data directly from  $\mathbf{Z}$ . In addition, prediction errors can be determined by arithmetic decoding, and the encrypted blocks can be recovered exactly. With  $K_P$  and  $K_M$ , the receiver conducts inverse block permutation and inverse block modulation, and the original image can be recovered losslessly.

### A. Image Encryption with Correlation Preservation

For VRAE, the image owner generates the encrypted image while preserving the original pixel correlation within each image blocks. The owner first divides the cover image  $\mathbf{X}$  into non-overlapping image blocks sized  $n = n_1 \times n_2$  as

$$x_i = (x_{i,1,1}, x_{i,1,2}, \dots, x_{i,2,1}, x_{i,2,2}, \dots, x_{i,n_1,n_2-1}, x_{i,n_1,n_2}), \quad (23)$$

where  $1 \leq i \leq N$ ,  $1 \leq j \leq n_1$ ,  $1 \leq k \leq n_2$ , and the amount of blocks is  $N = \lfloor N_1/n_1 \rfloor \times \lfloor N_2/n_2 \rfloor$ .

The owner then encrypts the image blocks using an improved pixel modulation algorithm that restores the pixel correlation. In previous scheme [23], traditional pixel modulation is conducted by first generating a random data sequence  $R = \{r_1, r_2, \dots, r_N\}$  of size  $N$  with an encryption key  $K_M$  and then modulating the pixels by (24).

$$x_{i,j,k}' = (x_{i,j,k} + r_i) \bmod 256. \quad (24)$$

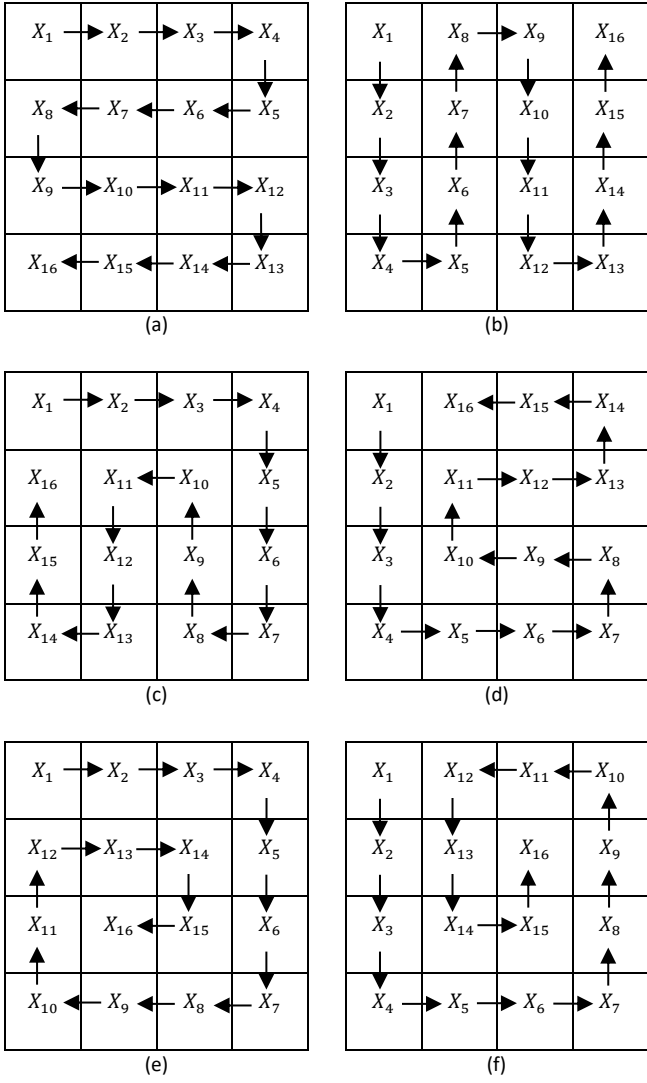


Fig.7 Possible arrangements of image blocks ( $N = 4 \times 4$ )

Denote the minimum and maximum value in  $X_i$  as  $\min(X_i)$  and  $\max(X_i)$ , respectively. When  $r_i \in [0, 255 - \max(X_i)] \cup (255 - \min(X_i), 255]$ , the difference value of any two pixels in the image block remains unchanged after the modulation.

$$x_{i,j_1,k_1}' - x_{i,j_2,k_2}' = x_{i,j_1,k_1} - x_{i,j_2,k_2}, j_1 \neq j_2 \text{ or } k_1 \neq k_2 \quad (25)$$

On the contrary, when  $r_i \in (255 - \max(X_i), 255 - \min(X_i)]$ , pixel correlation of image block will be affected. Take  $X_i = (202, 171, 166, 130)$  and  $r_i = 85$  as an example,  $\min(X_i) = 130$  and  $\max(X_i) = 202$ , the spatial correlation will be influenced when  $r_i \in (53, 125]$ . After pixel modulation, the pixel values become  $X_i' = (31, 0, 251, 215)$ . Therefore, traditional pixel modulation methods will inevitable change some differences between the adjacent pixels.

To decrease the influence of pixel modulation on the spatial correlation, we design an improved pixel modulation algorithm based on adjacent image block. Fig. 7 shows some possible arrangements of image blocks where  $N = 4 \times 4$ . Since there is a spatial relationship between two adjacent blocks, a previous block  $X_{i-1}$  is used to predict the ideal range of random data  $r_i$  for the pixel modulation of a current block  $X_i$ . Firstly,

according to  $\min(X_{i-1})$  and  $\max(X_{i-1})$ , the ideal range of  $r_{i-1}$  is  $[0, 255 - \max(X_{i-1})] \cup (255 - \min(X_{i-1}), 255]$ . The owner uses a scale factor as  $\zeta \in [0, 1]$  to restrict the range as  $[0, \zeta \cdot (255 - \max(X_{i-1}))] \cup (255 - \zeta \cdot \min(X_{i-1}), 255]$ . Then, by using  $r_i$  as the seed, the owner generates a new random integer  $r_i' \in [0, \zeta \cdot (255 - \max(X_{i-1}))] \cup (255 - \zeta \cdot \min(X_{i-1}), 255]$  for the pixel modulation of each image block  $X_i$  except the first block  $X_1$ , where the owner directly let  $r_1' = r_1$ . Thus, the traditional pixel modulation is updated in (26), and the random data sequence  $R' = \{r_1', r_2', \dots, r_N'\}$  is generated using the encryption key  $K_M$ .

$$x_{i,j,k}' = (x_{i,j,k} + r_i') \bmod 256. \quad (26)$$

The owner further permutes the modulated image blocks  $X_i'$  using the Arnold transformation, which can be described as:

$$\begin{bmatrix} k' \\ l' \end{bmatrix} = \begin{bmatrix} 1 & b \\ a & ab + 1 \end{bmatrix} \begin{bmatrix} k \\ l \end{bmatrix} \bmod(M), \quad (27)$$

where  $k$  and  $l$  is the row and column of the image block before transformation respectively,  $k'$  and  $l'$  represents the row and column after transformation,  $a$  and  $b$  is the transformation parameter, and  $M$  is the same number of image blocks on the row and column. If  $[N_1/n_1] \neq [N_2/n_2]$ ,  $M$  should be set to be greatest common factor of  $[N_1/n_1]$  and  $[N_2/n_2]$ . The parameters  $a$ ,  $b$  and  $M$  is determined by the encryption key  $K_P$ . To resist the known plaintext attacks, the image encryption should be one-time pad.

This way, the encrypted image with correlation preservation  $\mathbf{Y}$  can be generated and uploaded into the cloud.

### B. Data Embedding

In the cloud, the data hider embeds the additional data into the encrypted image, where the spatial redundancy in the plaintext image can be largely preserved by image encryption with block modulation and block permutation. The procedure of data embedding is composed of three steps: prediction-errors generation, entropy encoding of prediction-errors, and data embedding.

Firstly, the data hider divides  $\mathbf{Y}$  into non-overlapped blocks under the same principle of that in Section V. A. Since most image blocks preserves spatial correlation of the plaintext image blocks, for each block  $Y_i$ , one pixel  $y_{i,j_1,k_1}$  is selected as  $P_R$ . Then, the other pixels served as  $P_E$  can be predicted with adjacency prediction and MED predictor, the corresponding PEH is generated.

Secondly, with arithmetic coding, the owner finds out the optimal threshold  $T_{opt}$ , then compresses the prediction errors losslessly to obtain the compressed data  $CD$  and auxiliary data  $AD$ , and calculates  $L = \ell(CD) + \ell(AD)$ , which is transferred into  $\ell(L)$  bits binary data. Then, the data hider encrypts the additional data  $\mathbf{S}$  with data hiding key  $K_H$  to obtain  $\mathbf{S}'$ . The data to be embedded is composed of  $L$ ,  $CD$ ,  $AD$  and  $\mathbf{S}'$ .

Finally, the owner skips the reference pixels, and replaces each bit-planes one by one with the data to be embedded from LSB-plane to MSB-plane. As a result, the marked encrypted image  $\mathbf{Z}$  is generated.

### C. Data Extraction and Image Recovery

In the proposed VRAE-based RDHEI scheme, the procedure



Fig. 8. Six typical test images for the experiments

of data extraction and image recovery is also separable as the proposed VRBE-based RDHEI scheme. And the operation of data extraction is almost the same as that of VRBE.

Skipping the reference pixels, the receiver firstly extracts the first  $\ell(L)$  bits in the LSB-plane of  $\mathbf{Z}$ , which is the length  $L$  of  $CD$  and  $AD$  in the proposed VRAE method. Then, With  $L$ , the receiver can skip the reference pixels and the lower bit-planes carrying  $CD$  and  $AD$ , and extract the embedded data  $\mathbf{S}'$  from the higher bit-planes. Finally, the authorized receiver with data hiding key  $K_H$  decrypts  $\mathbf{S}'$  to obtain the additional data  $\mathbf{S}$  error-free.

As showed in Section III.D, the receiver can recover the encrypted image  $\mathbf{Y}$  losslessly. Without the encryption keys  $K_P$  and  $K_M$ , little detail of the original image can be discovered from  $\mathbf{Y}$ . With  $K_P$  and  $K_M$ , the receiver can further recover the original image. He firstly divides  $\mathbf{Y}$  into non-overlapped image blocks  $\{Y_1, Y_2, \dots, Y_N\}$  under the same principle of that in Section V. A. With the encryption key  $K_P$  and (28), the receiver operates inverse permutation of blocks  $\{Y_1, Y_2, \dots, Y_N\}$  to obtain the modulated image blocks  $\{X_1', X_2', \dots, X_N'\}$ .

$$\begin{bmatrix} k \\ l \end{bmatrix} = \begin{bmatrix} ab + 1 & -a \\ -b & 1 \end{bmatrix} \begin{bmatrix} k' \\ l' \end{bmatrix} \bmod(M). \quad (28)$$

Then, he further conducts the inverse pixel modulation by:

$$x_{i,j,k} = (x_{i,j,k}' - r_i') \bmod 256. \quad (29)$$

The inverse modulation is carried out in the order of  $\{X_1', X_2', \dots, X_{N-1}', X_N'\}$ . Firstly, the receiver generates the random data sequence  $R = \{r_1, r_2, \dots, r_N\}$  with encryption key  $K_M$ . Then, with  $r_1' = r_1$ ,  $X_1$  can be recovered from  $X_1'$  by using (29). With  $r_2$  and  $X_1$ ,  $r_2'$  can be generated to recover  $X_2'$ . This way, with recovered  $X_{i-1}$  and  $r_i$ , the other blocks  $X_i (i > 2)$  can be recovered subsequently, and so on. Finally, the original image  $\mathbf{X}$  is recovered error-free.

When the receiver has both the data hiding key and encryption keys, he is capable to not only extract the secret data exactly but also recover the cover image losslessly.

## VI. EXPERIMENTAL RESULTS

To verify the two RDHEI schemes in the proposed framework, we have conducted many experiments on thousands of gray-scaled images from typical image datasets, namely, UCID [38], BOSSBase [39], and BOWS-2 [40]. We use binary random sequences as additional messages, i.e., the possibilities for 0 and 1 are equal. Notice that in the figures and tables in this section, we are comparing the pure payload

between different methods, i.e., all parts of the side information required in the scheme are excluded from the total amount of the embedded data to calculate the net payload. For objective image quality evaluation, we employ the peak signal-to-noise ratio (PSNR) and structural similarity (SSIM) [41]. SSIM is proposed generally based on the degradation of structural information, which is much better in providing consistent and subjective image visual quality. The value of SSIM ranges from 0 to 1. A higher structure similarity between the cover image and the marked image is represented by a high SSIM closer to 1.

We firstly show the embedding performances of the proposed schemes, which includes redundancy preservation (only for VRAE), embedding capacity, reversibility, security and separability. Then, we compare the proposed RDHEI schemes with many state-of-the-art RDHEI methods proposed in [23] [32-36].

### A. Performance Analysis

In Fig.8, we select five examples of cover images for testing. Fig. 9. shows some experiment results of the proposed schemes on Lena, where (a) is the original image, (b) is the encrypted image with correlation preservation by block modulation and block permutation ( $n = 8 \times 8$ ,  $\zeta = 0.5$ ), (c) is the marked encrypted images of (b) based on PE-VRAE, (d) is the encrypted images with vacating room by arithmetic coding, (e) is the marked encrypted images of (d), and (f) is the same recovered original image from (c) or (e) independently. The data extraction is always successful, i.e., the bit-wise error rate (BER) between the decrypted extracted data and the original additional data is 0. The recovered image is identical to the original image, i.e., the SSIM between the recovered image and the original image is 1.

**Redundancy Preservation for PE-VRAE.** In PE-VRAE, the spatial correlation within each block can be influenced by the pixel modulation, which is related with the blocks size  $n = n_1 \times n_2$  and the scale factor  $\zeta$ . When the pixel values are added with the random seed, the two ideal cases are all processed pixels' values are within [0, 255] and all are larger than the ceiling value, which is 255. However, some processed pixels' value may be within [0, 255], others are larger than 255. We regard these pixels with less amount, which no more than or larger than 255, as abnormal pixels. The total amount of all abnormal pixels reflects the correlation preservation within the blocks. Table 2 shows the experimental results with different block size  $n = \{4 \times 4, 6 \times 6, 8 \times 8\}$  and  $\zeta = \{0.25, 0.50,$

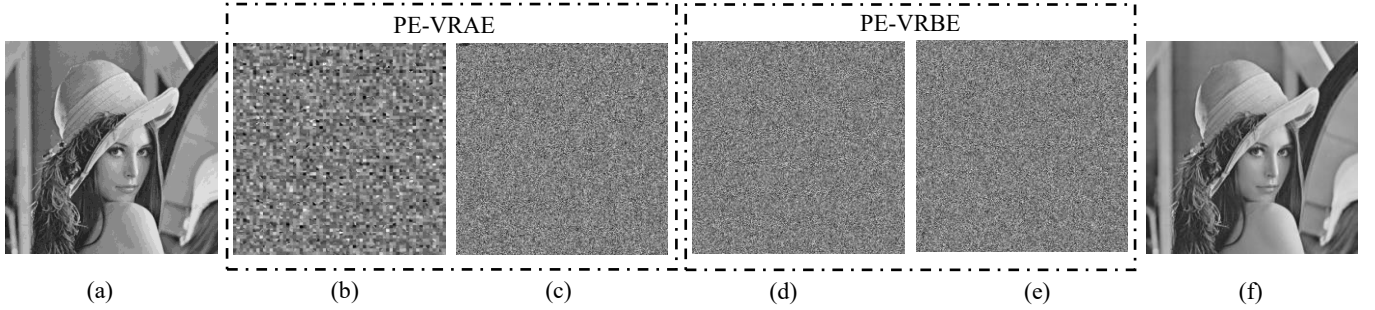


Fig. 9. Data embedding test. The original image cannot be directly observed from any of its encrypted versions. (a) Original image, (b) encrypted image of PE-VRAE, (c) marked encrypted image of PE-VRAE, (d) encrypted image of PE-VRBE, (e) marked encrypted image of PE-VRBE, (f) error-free recovered image

Table 2. The amount of abnormal pixels with different parameters

n	4×4					6×6					8×8					
	$\zeta$	0.25	0.50	0.75	1.00	None	0.25	0.50	0.75	1.00	None	0.25	0.50	0.75	1.00	None
Lena	0.25	1	194	649	1399	6336	5	263	1035	2100	7576	0	310	1524	2895	9508
Baboon	0.25	5	23	93	524	16323	10	33	129	418	17654	8	31	125	385	19610
Airplane	0.25	6	187	962	1842	6693	7	199	1037	2024	8668	14	377	1262	2085	10081
Tiffany	0.25	15	33	48	121	5266	6	7	19	100	5910	26	34	39	99	7252
Man	0.25	561	1041	1951	3799	30213	880	1443	2625	4689	37349	1065	1734	3047	5339	42889

Table 3. The maximal net payload with different parameters by the proposed PE-VRAE scheme (bpp)

n	4×4					6×6					8×8					
	$\zeta$	0.25	0.50	0.75	1.00	None	0.25	0.50	0.75	1.00	None	0.25	0.50	0.75	1.00	None
Lena	0.25	3.107	3.103	3.094	3.082	2.952	3.229	3.224	3.210	3.198	3.065	3.322	3.314	3.293	3.285	3.143
Baboon	0.25	1.498	1.497	1.494	1.475	1.195	1.576	1.574	1.570	1.559	1.259	1.625	1.624	1.621	1.610	1.288
Airplane	0.25	3.383	3.378	3.364	3.355	3.256	3.535	3.531	3.516	3.503	3.398	3.637	3.630	3.620	3.611	3.495
Tiffany	0.25	3.235	3.235	3.234	3.234	3.098	3.359	3.359	3.358	3.358	3.219	3.441	3.441	3.441	3.440	3.292
Man	0.25	2.747	2.745	2.741	2.731	2.558	2.859	2.858	2.851	2.843	2.658	2.940	2.937	2.931	2.923	2.742
Average	0.25	2.794	2.792	2.785	2.775	2.612	2.912	2.909	2.901	2.892	2.720	2.993	2.989	2.981	2.974	2.792

0.75, 1.00, none}, where “none” represents that we apply the traditional pixel modulation in [23] instead of our improved strategy. Given a block size, due to the interval expansion of random data for modulation, the amount of abnormal pixels increases along with the increase of  $\zeta$ , and the amount of abnormal pixels without  $\zeta$  to limit the interval of random data as [23] is much larger than that of proposed method with special  $\zeta$ . The test proves that our proposed pixel modulation strategy can largely reserve the spatial correlation within the image blocks, which plays a crucial role in ensuring a large payload.

**Embedding Capacity.** The embedding rate (ER) of Fig. (c) and (e) is 3.314bpp, 3.444bpp respectively.

Based on PE-VRAE, with different parameters  $n$  and  $\zeta$ , the achieved net payload of five test images after image encryption is showed in Table 3. With the same block size, due to the abnormal pixels’ influence in the precision of pixels prediction, the achieved embedding rate (ER) decreases gradually with the increase of  $\zeta$ , especially the average ER without using  $\zeta$  is over 0.1bpp less than that of  $\zeta = 1.00$ . With the same  $\zeta$ , higher ER can be achieved with larger block sizes. The reason

is that the amount of reference pixels decreases with the increase of block size, namely, the amount of prediction errors increases. Table 3 indicates that the ER of Lena, Airplane and Tiffany can be above 3bpp, the ER of Man is up to 2.9bpp. Even for textured images like Baboon, the ER can be 1.625bpp ( $n = 8 \times 8$ ,  $\zeta = 0.25$ ).

Table 4. The maximal net payload based on PE-VRBE (bpp)

Lena	Baboon	Airplane	Tiffany	Man	Average
3.444	1.710	3.804	3.562	3.060	3.116

Table 4 shows the achieved ER based on the proposed PE-VRBE scheme. The average embedding capacity of the five test images is 3.116bpp, which proves that the proposed scheme can hide a large amount of additional data within a cover image. Compared with Table 3, Table 4 indicates that the achieved ER of the proposed PE-VRBE scheme is higher than that of the proposed PE-VRAE scheme. One reason is that the PE-VRBE scheme uses the spatial redundancy of original plaintext image directly to vacate embedding room while the spatial redundancy

Table 5. The average PSNR (dB) and SSIM of five test images with different parameters by the proposed PE-VRAE scheme

Image	$n$	4×4					6×6					8×8				
		$\zeta$	0.25	0.50	0.75	1.00	None	0.25	0.50	0.75	1.00	None	0.25	0.50	0.75	1.00
Encrypted image	PSNR	13.25	13.70	13.54	12.90	9.38	13.28	13.66	13.52	12.94	9.41	13.03	13.38	13.27	12.79	9.33
	SSIM	0.305	0.390	0.366	0.280	0.073	0.357	0.434	0.430	0.352	0.086	0.336	0.395	0.388	0.323	0.090
Marked encrypted image	PSNR	9.48	9.53	9.53	9.50	9.30	9.45	9.46	9.47	9.44	9.36	9.39	9.40	9.40	9.40	9.32
	SSIM	0.046	0.045	0.044	0.045	0.043	0.043	0.044	0.044	0.041	0.043	0.042	0.041	0.044	0.041	0.042

Table 6. The average PSNR (dB) and SSIM of five test images by the proposed VRBE schemes

	Encrypted image						Marked encrypted image					
	Lena	Baboon	Airplane	Tiffany	Man	Average	Lena	Baboon	Airplane	Tiffany	Man	Average
PSNR	9.23	9.52	8.01	6.88	7.99	8.33	9.23	9.51	8.01	6.90	8.00	8.33
SSIM	0.034	0.032	0.035	0.039	0.068	0.041	0.036	0.029	0.034	0.038	0.068	0.041

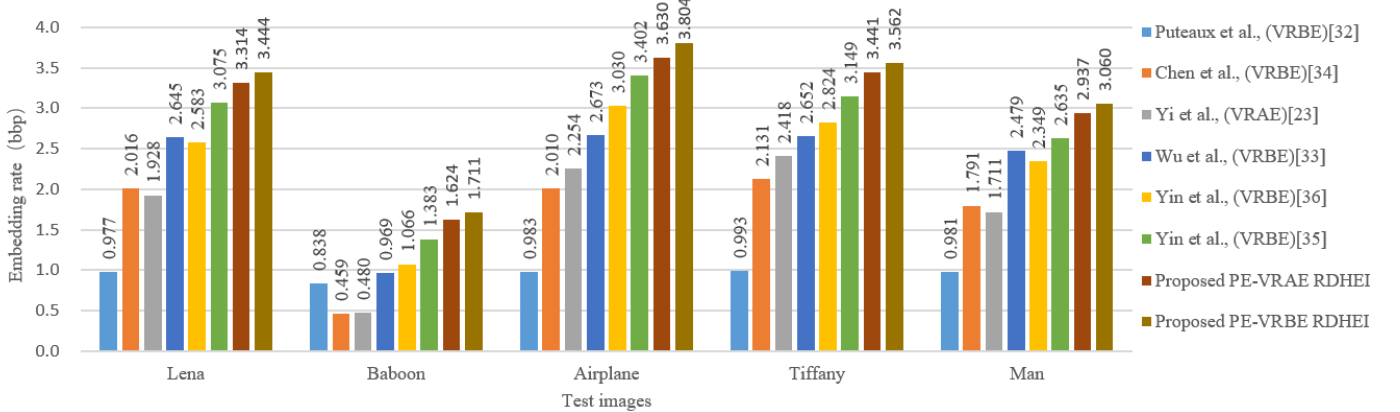


Fig.10. Comparison of ER on five test images between the proposed schemes and six state-of-the-art RDHEI methods

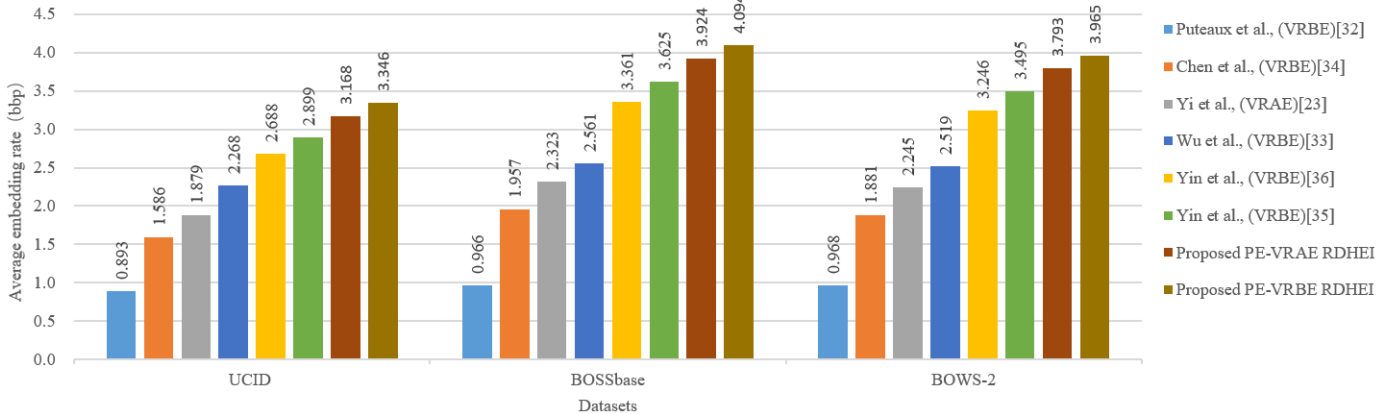


Fig. 11. Comparison of average ER on three image datasets between the proposed schemes and six state-of-the-art RDHEI methods

is somewhat degraded during image encryption for PE-VRAE, and another is that there is only one reference pixel for PE-VRBE while the number of reference pixels for PE-VRAE is equal to the number of image blocks.

**Security.** Table 5 and Table 6 show the average PSNR (dB) and SSIM of five test images by the proposed PE-VRAE scheme with different parameters and by the proposed PE-VRBE scheme, respectively, where the PSNRs and SSIMs are calculated between the original image and the processed images generated in different phases by the owner or the data hider.

In PE-VRAE schemes, the average PSNR and SSIM values between the original image and its encrypted version of five test images vary with different parameters  $n$  and  $\zeta$ . Although there is blocking artifact during block modulation and block permutation, the effect of the proposed encryption for VRAE is reasonable. With different entropy encodings, parameters  $n$  and  $\zeta$ , the average PSNR and SSIM between the original image and the marked encrypted image have no significant difference, which are very low, i.e., about 9.30 dB and 0.04. Even without data encryption of entropy encoding, just the encrypted image

can be recovered from the marked encrypted image. With one-time pad during image encryption, the proposed VRAE-based schemes can resist the known plaintext attacks well. Therefore, after image encryption and data embedding, there is no leakage of original image content in the marked decrypted image, and high security is verified.

From Table 6, the PSNR and SSIM values between the original image and its encrypted versions are very low in the proposed PE-VRBE schemes. The average PSNR between the original image and the encrypted image with vacated room is 8.32dB, and the SSIM is 0.041. The data embedding in the encryption domain does not influence the encryption effect. Since the data of entropy encoding is encrypted during image encryption, contour lines of the original image can no longer be detected from the encrypted versions. Therefore, after image encryption and data embedding, little detail of the cover image can be discovered from the encrypted versions.

**Separability & Reversibility.** In the proposed schemes, the receiver gets different contents according to his authentication. The receiver only with the data hiding key can extract the hidden data exactly without knowing any information about the original content, and the data extraction is always successful, i.e., the bit-wise error rate (BER) between the extracted decrypted data and the original additional data is 0. Similarly, the receiver with only the encryption keys cannot obtain the hidden data, but he can recover the original image losslessly. The recovered image is identical to the original image, i.e., Fig. 9(f) is identical to Fig. 9(a). In the experiments, the PSNRs and SSIMs between the recovered images and the original images are  $+\infty$  and 1, respectively. The above experiments demonstrate the separability and reversibility of the proposed schemes.

### B. Comparison with State-of-the-art RDHEI Scheme

We compare the proposed schemes with many state-of-the-art RDHEI schemes [23] [32-36]. We compare the embedding rate of these schemes when the average PSNR of the marked encrypted image produced by the schemes are close. Therefore, a larger average embedding rate means a better embedding performance.

In the experimental settings, the parameters  $\alpha$  and  $\beta$  in [23] and [33] are set as 5 and 2 respectively. In [32], we accept the EPE-HCRDH scheme, which can achieve a higher embedding capacity. In [34], the length of fixed-length codewords is set as 3 and the block size is set to  $4 \times 4$ . In [35], the 8 bit-plants of prediction errors are rearranged and compressed. In [36], the codewords are predefined as  $\{00, 01, 100, 101, 1100, 1101, 1110, 11110, 11111\}$  to represent nine kinds of the multi-MSB prediction. In the proposed PE-VRAE scheme, we set  $n = 8 \times 8$  and  $\zeta = 0.50$ .

**Average Performance.** Fig. 10 provides the performance comparison of embedding rate between the proposed schemes and [23] [32-36]. The embeddings are conducted on the cover images shown in Fig. 8. The achieved embedding rates of EPE-HCRDH [32] on these images are lower than 1 bpp. The reason is that the method merely uses the MSB of each pixel for data embedding. Chen et al. [34] can provide a higher embedding capacity. However, the method performs poorly on textured

images, e.g., 0.459 bpp on Baboon. Yi et al. [23] provides a similar embedding performance compared to [34], where the net payload on Baboon is 0.480 bpp. [33] [35-36] can achieve higher payloads on both flat and textured images. For example, the embedding capacity of [35] is 3.075 bpp, 1.383 bpp, 3.402 bpp, 3.149 bpp and 2.635 bpp on Lena, Baboon, Airplane, Tiffany and Man respectively. By comparison, the proposed schemes outperform above methods in net payload. With the proposed VRAE-based method by arithmetic encoding, the ER is up to 3.314 bpp, 1.624 bpp, 3.630 bpp, 3.441 bpp and 2.937 bpp in Lena, Lena, Baboon, Airplane, Tiffany and Man respectively. While with the proposed VRBE-based method, the ER is up to 3.444 bpp, 1.711 bpp, 3.804 bpp, 3.562 bpp and 3.060 bpp in five test image respectively. The reason is that the proposed schemes not only take full advantage of spatial redundancy in the plain-text image, but also improve the performance of entropy coding with arithmetic encoding. Apart from the five typical images, we further analyze the average embedding performance on UCID [38], BOSSBase [39], and BOWS-2 [40]. Fig. 11 reports the performances of average embedding rate on the three datasets. While [35] can embed a larger payload into the cover image than [23, 32-34, 36], the proposed scheme can further offer a larger net payload. The experiment results demonstrate that the proposed schemes outperform other competitors. For example, the average net payload of the proposed VRBE-based scheme on UCID, BOSSbase 1.01 and BOWS-2 is 3.346 bpp, 4.094 bpp and 3.965 bpp, which is 15.41%, 12.94% and 13.45% larger than that of [35] under the same category, respectively. While, the average net payload of the proposed PE-VRAE scheme with arithmetic encoding on UCID, BOSSbase 1.01 and BOWS-2 is 3.168 bpp, 3.924 bpp and 3.793 bpp, which is respectively 68.60%, 68.92% and 68.95% larger than that of [23] under the same category.

## VII. EXTENSION

In this section, we replace the arithmetic encoding in the proposed embedding room generation algorithm with Huffman encoding to verify the adaptiveness of the proposed framework. Huffman code is another common entropy encoding paradigm. Differing from arithmetic coding which encodes the entire pixels into a single number, Huffman encoding replaces each independent encoding pixel with an independent code and all jointly encoding pixels with a same code.

For a given  $T \in [1, 255]$ , we can build an optimal Huffman tree  $\mathfrak{h}$  with codewords  $\{C_{-T}, C_{-T+1}, \dots, C_{-1}, C_0, \dots, C_{T-2}, C_{T-1}, C_J\}$ . We assign the independent encoding bins each with an independent codeword, and the joint encoding bins with a same codeword. The codewords of the independent encoding pixels are  $\{C_{-T}, C_{-T+1}, \dots, C_{-1}, C_0, \dots, C_{T-2}, C_{T-1}\}$  with length  $\ell(C_e)$  ( $e \in [-T, T-1]$ ) bits, and that of the jointly encoding pixels is  $C_J$  with length  $\ell(C_J)$  bits.

For the image decompression, we need to record the information for constructing the Huffman tree, including the threshold  $T$ , the  $(2T+1)$  codewords and the length of each codeword. For  $T \in [1, 255]$ , it can be expressed within eight bits. Since the maximum length of each pixel is less than eight, the length of each codeword should be less than eight so that

every embedding pixel can accommodate its codeword to vacate embedding room. The length of each codeword can be represented within three bits, appended with its corresponding binary codeword. The above side information is concatenated as a binary sequence with length  $\ell_T(CD_1)$  as

$$\ell_T(CD_1) = 8 + 3(2T+1) + \sum_{e=-T}^{T-1} \ell(C_e) + \ell(C_J) \quad (30)$$

For each *embedding pixel*  $y_{i,j,k}$  ( $1 \leq i \leq N, j \neq j_1$  or  $k \neq k_1$ ), its prediction error  $e_{i,j,k}$  can be represented by its corresponding Huffman codeword  $c_{i,j,k}$ . When  $e_{i,j,k} \in [-T, T-1]$ , the codeword  $c_{i,j,k}$  is  $C_{e_{i,j,k}}$ , otherwise the codeword  $c_{i,j,k}$  is  $C_J$ . Given a  $T$ , total length of codewords used for recording the prediction errors is defined in (31).

$$\ell_T(CD_2) = \sum_{e=-T}^{T-1} h_e \cdot \ell(C_e) + h_J \cdot \ell(C_J). \quad (31)$$

Then,  $CD_1$  is appended with  $CD_2$ , we have

$$\ell_T(CD) = \ell_T(CD_1) + \ell_T(CD_2) = 8 + 3(2T+1) + \ell_T(CD') \quad (32)$$

where,

$$\ell_T(CD') = [\sum_{e=-T}^{T-1} (h_e + 1) \ell(C_e) + (h_J + 1) \ell(C_J)]. \quad (33)$$

With Huffman encoding, the embedding capacity of vacated room in (9) can be described as

$$EC_T = 8 \cdot (\sum_{e=-T}^{T-1} h_e - 1) - 3(2T+1) - \ell(L) - \ell_T(CD') \quad (34)$$

Then, to achieve maximal embedding capacity, optimal thresholds  $T_{opt}$  should satisfy

$$T_{opt} = \operatorname{argmax}_{T \in [1, 255]} EC_T$$

$$\text{w.r.t. } \forall \ell(C_e) \leq 8, \ell(C_J) \leq 8, e \in [-T, T-1] \quad (35)$$

For a special  $T$ , the value of the first three items in (34) is fixed, the optimal Huffman tree should be constructed to minimize the value of  $\ell(CD')$ , i.e.,

$$h_T = \operatorname{argmin} \ell(CD')$$

$$\text{w.r.t. } \forall \ell(C_e) \leq 8, \ell(C_N) \leq 8, e \in [-T, T-1] \quad (36)$$

For each prediction-error value  $e \in B_e$ , the occurrence probability of its codeword  $C_e$  is

$$p(C_e) = (h_e + 1) / (\sum_{e=-255}^{255} h_e + 2 \cdot T + 1). \quad (37)$$

where,

$$\sum_{e=-255}^{255} h_e = N \cdot (n_1 \cdot n_2 - 1). \quad (38)$$

The total occurrence probability of codeword  $C_J$  for all  $P_J$  is

$$p(C_J) = 1 - \sum_{e=-T}^{T-1} p(C_e). \quad (39)$$

Based on the probability distribution, a Huffman tree can be generated for special threshold  $T$ . By trying all possible  $T$ , the optimal thresholds  $T_{opt}$  can be determined with (35). This way, the  $T_{opt}$  and its corresponding optimized Huffman tree is generated, and the prediction errors can be compressed with Huffman encoding to vacate embedding room.

In PE-VRAE ( $n = 8 \times 8$ ,  $\zeta = 0.25$ ), the achieved ER of Lena, Baboon, Airplane, Tiffany and Man by Huffman encoding is  $3.187\text{bpp}$ ,  $1.454\text{bpp}$ ,  $3.497\text{bpp}$ ,  $3.306\text{bpp}$  and  $2.817\text{bpp}$  respectively, while the average achieved ER on UCID [38], BOSSBase [39], and BOWS-2 [40] by Huffman encoding is respectively  $3.043\text{bpp}$ ,  $3.625\text{bpp}$  and  $3.669\text{bpp}$ . These

experimental data is a bit lower than that of PE-VRAE with arithmetic coding, but higher than that of [23] [32-36]. With PE-VRBE by Huffman encoding, the achieved ER of Lena, Baboon, Airplane, Tiffany and Man is  $3.317\text{bpp}$ ,  $1.535\text{bpp}$ ,  $3.657\text{bpp}$ ,  $3.427\text{bpp}$  and  $2.944\text{bpp}$  respectively, the average achieved ER on UCID [38], BOSSBase [39], and BOWS-2 [40] is  $3.217\text{bpp}$ ,  $3.952\text{bpp}$  and  $3.814\text{bpp}$  respectively. These experimental data is a bit lower than that of PE-VRBE with arithmetic coding, but also higher than that of [23] [32-36], indicating that the Huffman encoding is also fit to the proposed framework of RDHEI.

In addition, we prove that applying different entropy encoding methods has little or no effect on the security, separability and reversibility of the proposed RDHEI schemes. More efficient entropy encoding methods can be developed to be used in the proposed framework to achieve higher ER.

## VIII. CONCLUSION

This paper proposes a framework for high-capacity reversible data hiding in encrypted images (RDHEI) for both VRAE and VRBE cases using pixel predictions and entropy encoding. We propose an embedding room generation algorithm to produce vacated room by generating the prediction-error histogram of the selected cover using adjacency prediction and the median edge detector. We then propose a VRBE scheme that generate the embedding room using the proposed algorithm, and encrypt the preprocessed image by using the stream cipher with two encryption keys. We further propose a scheme that involves an improved block modulation and permutation encryption algorithm where the spatial redundancy in the plain-text image can be largely preserved. Then the proposed embedding room generation algorithm is applied on the encrypted image. At the data hider's side of both the schemes, the data hider locates the embedding room and embeds the encrypted additional data. The receivers with different authentication can respectively conduct error-free data extraction and/or error-free image recovery. Experimental results prove the effectiveness of the proposed schemes on typical image datasets. While many previous works cannot provide large embedding rate on textured images like Baboon, the proposed scheme can provide the data hider with up to  $1.711\text{bpp}$  payload.

## REFERENCES

- [1] J. Tian, "Reversible data embedding using a difference expansion," *IEEE Trans. Circuits Syst. Video Technol.*, vol. 13, no. 8, pp. 890–896, Aug. 2003.
- [2] A. M. Alattar, "Reversible watermark using the difference expansion of a generalized integer transform," *IEEE Trans. Image Process.*, vol. 13, no. 8, pp. 1147–1156, Aug. 2004.
- [3] X. Wang, X. Li, B. Yang, and Z. Guo, "Efficient generalized integer transform for reversible watermarking," *IEEE Signal Process. Lett.*, vol. 17, no. 6, pp. 567–570, Jun. 2010.
- [4] Y. Qiu, Z. Qian, and L. Yu, "Adaptive reversible data hiding by extending the generalized integer transformation," *IEEE Signal Process. Lett.*, vol. 23, no. 1, pp. 130–134, Jan. 2016.
- [5] Z. Ni, Y. Shi, N. Ansari, and W. Su, "Reversible data hiding," *IEEE Trans. Circuits Syst. Video Technol.*, vol. 16, no. 3, pp. 354–362, Mar. 2006.

[6] X. Li, B. Li, B. Yang, and T. Zeng, "General framework to histogram-shifting-based reversible data hiding," *IEEE Trans. Image Process.*, vol. 22, no. 6, pp. 2181–2191, Jun. 2013.

[7] B. Ou and Y. Zhao, "High capacity reversible data hiding based on multiple histograms modification," *IEEE Trans. Circuits Syst. Video Technol.*, vol. 30, no. 8, pp. 2329–2342, Aug. 2020.

[8] W. Qi, X. Li, T. Zhang, and Z. Guo, "Optimal Reversible Data Hiding Scheme Based on Multiple Histograms Modification," *IEEE Trans. Circuits Syst. Video Technol.*, vol. 30, no. 8, pp. 2300–2312, Aug. 2020.

[9] X. Zhang, "Reversible data hiding with optimal value transfer," *IEEE Trans. Multimedia*, vol. 15, no. 2, pp. 316–325, Feb. 2013.

[10] W. Zhang, X. Hu, X. Li, and N. Yu, "Optimal transition probability of reversible data hiding for general distortion metrics and its applications," *IEEE Trans. Image Process.*, vol. 24, no. 1, pp. 294–304, Jan. 2015.

[11] D. Hou, W. Zhang, Y. Yang, and N. Yu, "Reversible data hiding under inconsistent distortion metrics," *IEEE Trans. Image Process.*, vol. 27, no. 10, pp. 5087–5099, Oct. 2018.

[12] F. Huang, X. Qu, H. J. Kim, and J. Huang, "Reversible data hiding in JPEG images," *IEEE Trans. Circuits Syst. Video Technol.*, vol. 26, no. 9, pp. 1610–1621, Sep. 2016.

[13] Y. Qiu, H. He, Z. Qian, S. Li, and X. Zhang, "Lossless Data Hiding in JPEG Bitstream Using Alternative Embedding," *J. Vis. Commun. Image Represent.*, vol. 52, pp. 86–91, 2018.

[14] Y. Qiu, Z. Qian, H. He, H. Tian, and X. Zhang, "Optimized lossless data hiding in JPEG bitstream and relay transfer based extension," *IEEE Trans. Circuits Syst. Video Technol.*, vol. 31, no. 4, pp. 1380–1394, Apr. 2021.

[15] Y. Du, Z. Yin, and X. Zhang, "High capacity lossless data hiding in JPEG bitstream based on general VLC mapping," *IEEE Trans. Depend. Secure Comput.*, doi: 10.1109/TDSC.2020.3013326.

[16] W. Puech, M. Chaumont, O. Strauss, A reversible data hiding method for encrypted images, in Proc. SPIE, vol. 6819, Mar. 2008.

[17] X. Zhang, Reversible data hiding in encrypted image, *IEEE Signal Process. Lett.*, vol. 18, no. 4, pp. 255–258, Apr. 2011.

[18] W. Hong, T. S. Chen, and H. Y. Wu, "An improved reversible data hiding in encrypted images using side match," *IEEE Signal Process. Lett.*, vol. 19, no. 4, pp. 199–202, Apr. 2012.

[19] J. Zhou, W. Sun, L. Dong, X. Liu, O. C. Au, and Y. Y. Tang, "Secure reversible image data hiding over encrypted domain via key modulation," *IEEE Trans. Circuits Syst. Video Technol.*, vol. 26, no. 3, pp. 441–452, Mar. 2016.

[20] X. Zhang, "Separable reversible data hiding in encrypted image," *IEEE Trans. Inf. Forensics Secur.*, vol. 7, no. 2, pp. 826–832, Apr. 2012.

[21] Z. Qian and X. Zhang, "Reversible data hiding in encrypted images with distributed source encoding," *IEEE Trans. Circuits Syst. Video Technol.*, vol. 26, no. 4, pp. 636–646, Apr. 2016.

[22] X. Zhang, J. Long, Z. Wang and H. Cheng, "Lossless and reversible data hiding in encrypted images with public key cryptography," *IEEE Trans. Circuits Syst. Video Technol.*, vol. 26, no. 9, pp. 1622–1631, Sept. 2016.

[23] S. Yi and Y. Zhou, "Separable and reversible data hiding in encrypted images using parametric binary tree labeling," *IEEE Trans. Multimedia*, vol. 21, no. 1, pp. 51–64, Jan. 2019.

[24] L. Qu, F. Chen, S. Zhang, and H. He, "Cryptanalysis of reversible data hiding in encrypted images by Block Permutation and Co-Modulation," *IEEE Trans. Multimedia*, doi: 10.1109/TMM.2021.3090588.

[25] K. Ma, W. Zhang, X. Zhao, N. Yu, and F. Li, "Reversible data hiding in encrypted images by reserving room before encryption," *IEEE Trans. Inf. Forensics Secur.*, vol. 8, no. 3, pp. 553–562, Mar. 2013.

[26] W. Zhang, K. Ma, and N. Yu, "Reversibility improved data hiding in encrypted images," *Signal Process.*, vol. 94, no. 1, pp. 118–127, Jan. 2014.

[27] D. Xu and R. Wang, "Separable and error-free reversible data hiding in encrypted images," *Signal Process.*, vol. 123, pp. 9–21, Jun. 2016.

[28] X. Cao, L. Du, X. Wei, D. Meng, and X. Guo, "High capacity reversible data hiding in encrypted images by patch-level sparse representation," *IEEE Trans. Cybern.*, vol. 46, no. 5, pp. 1132–1143, May 2016.

[29] S. Xiang and X. Luo, "Reversible data hiding in homomorphic encrypted domain by mirroring ciphertext group," *IEEE Trans. Circuits Syst. Video Technol.*, vol. 28, no. 11, pp. 3099–3110, Nov. 2018.

[30] Y. Qiu, Z. Qian, H. Zeng, X. Lin, and X. Zhang, "Reversible data hiding in encrypted images using adaptive reversible integer transformation," *Signal Process.*, vol. 167, pp. 1–10, Jan. 2020.

[31] Y. Qiu, Q. Ying, X. Lin, Y. Zhang, and Z. Qian, "Reversible data hiding in encrypted images with dual data embedding," *IEEE Access*, vol. 8, pp. 23209–23220, Jan. 2020.

[32] P. Puteaux and W. Puech, "An efficient MSB prediction-based method for high-capacity reversible data hiding in encrypted images," *IEEE Trans. Inf. Forensics Secur.*, vol. 13, no. 7, pp. 1670–1681, Jul. 2018.

[33] Y. Wu, Y. Xiang, Y. Guo, J. Tang, and Z. Yin, "An improved reversible data hiding in encrypted images using parametric binary tree labeling," *IEEE Trans. Multimedia*, vol. 22, no. 8, pp. 1929–1938, Aug. 2020.

[34] K. Chen and C. C. Chang, "High-capacity reversible data hiding in encrypted images based on extended Run-Length coding and block based MSB plane rearrangement," *J. Vis. Commun. Image Represent.*, vol. 58, pp. 334–344, Jan. 2019.

[35] Z. Yin, Y. Peng, and Y. Xiang, "Reversible data hiding in encrypted images based on pixel prediction and bit-plane compression," *IEEE Trans. Depend. Secure Comput.*, doi: 10.1109/TDSC.2020.3019490.

[36] Z. Yin, Y. Xiang, and X. Zhang, "Reversible data hiding in encrypted images based on multi-MSB prediction and Huffman encoding," *IEEE Trans. Multimedia*, vol. 22, no. 4, pp. 874–884, Apr. 2020.

[37] I. C. Dragoi and D. Coltuc, "On the Security of Reversible Data Hiding in Encrypted Images by MSB Prediction," *IEEE Trans. Inf. Forensics Secur.*, vol. 16, pp. 187–189, Jul. 2021.

[38] G. Schaefer and M. Stich, "UCID: An uncompressed color image database," in *Proc. Storage Retrieval Methods Appl. Multimedia*, vol. 5307. Bellingham, WA, USA: SPIE, 2003, pp. 472–481.

[39] P. Bas, T. Filler, and T. Pevn'y, "Break our steganographic system: The ins and outs of organizing boss," in *Proc. Int. Workshop Inf. Hiding*, 2011, pp. 59–70.

[40] P. Bas and T. Furon, "Image database of bows-2," 2017. [Online]. Available at <http://bows2.ec-lille.fr/>.

[41] Z. Wang, A. C. Bovik, H. R. Sheikh, and E. Simoncelli, "Image quality assessment: from error visibility to structural similarity," *IEEE Trans. Image Process.*, vol. 13, no. 4, pp. 600–612, Apr. 2004.